Optics and Laser Technology 121 (2020) 105779

Contents lists available at ScienceDirect

Optics and Laser Technology

journal homepage: www.elsevier.com/locate/optlastec

Full length article

Refractive index sensor based on evanescent field effects in hollow core PCF for detection of analytes over extended E + S + C + L + U communication bands

A. Dixit[a,b], S. Tiwari[a,c], U. Ramani[a], P.C. Pandey[a,*]

[a] Department of Physics, Indian Institute of Technology (BHU), Varanasi 221005, India
[b] Muzaffarpur Institute of Technology, Muzaffarpur 842003, India
[c] SOET, CMR University, Bangalore 562149, India

HIGHLIGHTS

- This work presents a new kind of asymmetric photonic crystal fiber.
- The birefringence and effective area of fiber have been utilized for sensing.
- This fiber shows better performance in dispersion compensation.

ARTICLE INFO

Keywords:
Single mode PCF
Analyte
Evanescent field sensing

ABSTRACT

We present an innovative platform for photonic crystal fiber (PCF) based refractive index (RI) sensor for the detection of analytes. Our PCF operating on the principle of a single mode is spliced with multi-mode fiber on both sides. This PCF contains an empty core, surrounded by elliptical plasma dielectric rods suspended in solid microstructured cladding for different pump signals over the extended range of E + S + C + L + U communication bands. The empty core of this photonic device is injected with analytes leading to generation of an evanescent field. The doping of boron is subjected to significantly diminish the upgraded refractive index of silica which ingresses special capabilities that endow an outstanding potential to PCF for the profoundly intense pulse laser. We present structure with over the extended E-band (1360-1460 nm) ultra-flat anomalous dispersion below −50 ps/nm/km and over the ultra-long U-band (1625–1675 nm) flat near zero anomalous dispersion with high birefringence dedicated to sensing application over the entire communication band. Our designed PCF shows better performance for both high contribution and asymmetric shape of plasma dielectric rods and is strongly sensitive to the refractive index of analytes injected in the core of the PCF.

1. Introduction

The refractive index (RI) sensor based on photonic crystal fiber (PCF) is an established new technology and offers a huge potential for detection of chemical and biological substances [1–3]. Currently, used all-solid photonic band gap (PBG) fiber is drawn on the same material for core and background cladding and mounts limitations on the real-life application. However, PCF in which solid core is replaced by hollow core would greatly extend the range of potential application. In contrast to all solid-PCF, the hollow core photonic crystal fiber (HCPCF)is not so common and offers more promising application in developing sensing devices, with the outstanding example of a biosensor, which is receiving substantial regard [4] in medical science. These fibers include the ability for the injection of various analytes into the hollow core sections of the PCF. The mode field in HCPCFs can barely reach beyond the cladding part due to the powerful containment of the optical field in the central hollow air core. The drawing of regular hollow core PCF with different pattern of dielectric rods is challenging due to the re-crystallization of glasses in multiple thermal processing. On the other hand, such photonic crystal fibers (PCF_S) enable full control over signals overlapping which can be configured and built up by analyte present in empty core and plasma dielectric rods suspended in the solid cladding. In the HCPCF biosensor, the two signals overlapping can be configured and built up by the core mode as the reference signal and the

* Corresponding author.
E-mail address: pcpandey.app@iitbhu.ac.in (P.C. Pandey).

https://doi.org/10.1016/j.optlastec.2019.105779
Received 28 February 2019; Received in revised form 4 August 2019; Accepted 16 August 2019
Available online 11 September 2019

cladding mode as the sensing signal.

The method used for optical fiber based sensors is not applicable to PCF based sensors due to the complex distribution of suspended dielectric rods and high refractive index abnormality existing between core & cladding materials. PCFs show photonic bandgap guidance as well as total internal reflection (TIR) for light guidance whereas conventional optical fibers work on the principle of TIR only. Numerous elaborated methods have been developed for the demonstration of RI sensing device based on normal photonic crystals, such as effective index method [5], transfer matrix method [6], finite element method [7], plane wave expansion method [8,9], and finite difference method [10,11]. Out of these various methods, finite difference method [FDM] is widely used in mode analysis of a Gaussian modulated beam in dielectric media and is sufficient for RI sensing by determining cladding mode with high-precision. This method is universal, well tested and methodologically simple. The major disadvantages of this method are, it is time-consuming and requires spacious treatment of boundaries.

H. Qu et al. reviewed liquid-filled Bragg fiber resonant sensors that use the principles of low-refractive-index contrast with experimental sensitivity of the proposed sensor comparable to ~1400 nm/RIU of those waveguide-based plasmonic sensors [12]. Different compact devices based on surface Plasmon resonance, evanescent field effect are perspective for chemical sensor with various structures including symmetrical dual D-shape fiber structure [13], diamond ring fiber structure [14], hollow core conventional fiber structure [15], cladding-off fiber structure [3], plasmonic material based PCF structure [16] and gold-coated PCF structure [17] based on surface plasmon resonance sensor. The development of temperature sensor based on high-birefringence PCF spliced with a fiber loop mirror was already demonstrated experimentally [18]. The output of this sensor is a measurement of transmission intensity and resonant dips with temperature and their quite dependence of the refractive index of the filled alcohol. Silica PCF interferometers containing a coating of an ultrathin layer of a Bovine Serum Albumin based on no adiabatic tapered fibers has been experimentally reviewed for fast detection of hydrogen concentration and accurate determination of optimized taper sensing length [19]. Its fabrication includes the steps of fiber heating and stretching. The waist thickness of the taper is reduced until dielectric rods collapsed, resulting in diameter of solid fiber less than optimized dimension (44 μm).

For the design of the PCF based sensor, different compositions of glasses were used which give an extension of flattened dispersion with a small effective area over a wide range of communication bands. However, being a strong role of material dispersion over the O + E band (1260–1460 nm), the asymmetric PCF is unable for compensating dispersion over these communication bands. The compatibility of the empty core PCF to confine and guide ultrahigh high-intense laser pulses without dispersion has been extended from the visible to infrared range. Flattened anomalous dispersion close to $-98.3\,\mathrm{ps{\cdot}nm^{-1}{\cdot}km^{-1}}$ was reported over the span of S + C + L communication bands [20]. A defected-core microstructured optical fiber (DCMF) in [21] was reported which shows an ultra flattened negative dispersion of about $-179\,\mathrm{ps{\cdot}nm^{-1}{\cdot}km^{-1}}$over S + C + L + U communications bands, varying from 1480 nm to 1675 nm. More recently, a new design of PCF structure exhibits an ultra flattened negative dispersion commencing from −201 to $-212\,\mathrm{ps{\cdot}nm^{-1}{\cdot}km^{-1}}$ pumped at communication bands over E + S + C + L + U range by using a small germanium doped core, has been reported by other groups as well [22]. Tee et al. proposed a PCF-in-PCF structure to compensate residual dispersion arising between −449.1 ps/nm/km to −461.8 ps/nm/km over the complete range of E + S + C + L + U communications bands [23]. Suitable percentage composition of these doped materials can also control dispersion-enhanced by intensity variation. However, all these computational analyses were done on different structures of PCF containing air-dielectric rods, rendering the usefulness of such an approach for the polarization issue questionable. Mostly used materials in the synthesis of the photonic crystal have the property to show a high refractive index for intense field and are thus perfectly unsuitable. We use doping of B_2O_3 in silica which provides a remarkable modulation of the refractive index of the composite materials. Furthermore, for RI sensing of bio-substance, we adopt the finite difference technique to solve nonlinear wave equation traveling in the hexagonal hollow core of the PCF. In comparison to normal PCF made of pure silica, our PCF containing doping of boron in the silica exhibits lower refractive index of the substrate. So, this type of doping is fit for the intense field and gives answers to basic questions regarding dispersion compensation which is significantly reduced in fiber made of these materials.

The PCF supports wave propagation in two distinct ways, mostly determined by arrangement pattern of dielectric rods; index-guiding PCF and photonic band gap PCF. The index-guiding PCF peruse the high refractive index of the core in comparison to the refractive index of the cladding and a reverse situation happens in case of the PBG guiding PCF. The background material used in the design of the core and cladding of normal PCF is silica. The confinement of ultra-high power femtosecond pulses by a periodic distribution of dielectric rods within a silica glass matrix has allowed the remarkable formation of full off-axis PBG. The refractive index of the cladding is reduced by filling of air in the dielectric rods, which runs longitudinally along the length of the fiber. The best confinement of light through photonic band gap occurs in the hollow core of the PCF. Due to hollow core, the refractive index of the core becomes low in comparison to the effective refractive index of the cladding. This mismatch of index properties of both zones creates a forbidden zone of energies in which a range of specific photons cannot be accommodated. The range of wavelengths that fall within the PCF's banned zone cannot travel out and thus remain confined to the low index hollow core. Our designed hollow core PCF can potentially break limits imposed by solid core PCF due to confinement of light in hollow core which is not the case in transparent solid materials. Another key point of selecting this PCF is that we can dynamically suffix materials, for example, chemicals into the hollow core. These materials inserted at different optical lengths, and at the center of the hollow core effectively enhance the refractive index of the core. The light guidance in the overlapped area depends on the effective refractive index of the materials covering it. If the overlapped region demonstrates high refractive index profile, then light confinement will be by total internal reflection (TIR) or in vice versa case by the photonic band gap.

This work has two objectives. First is to clearly define and demarcate the communication of high power laser beam inside an HCPCF-based sensor containing elliptical plasma dielectric rods. The detection process includes all relevant properties of the cladding modes using finite difference method under analytical boundary condition. Second is to demonstrate RI sensing of the designed PCF by inserting analytes in the hollow core as a point defect. The last section is the conclusion.

2. Evanescent field based PCF biosensor

This section presents recent developments and our review on the current principles of sensing with evanescent field based on solid-core, and hollow-core single mode PCF. The basic principle is to repel as much of the light intensity launched in the core into the surrounding part of the cladding. This usually happens in the case of solid-core PCF. Furthermore, the single mode operation which is conclusive for collecting phase information can be easily achieved using small solid-core PCF. The performance of evanescent field interaction in hollow core PCF can be improved when the analyte is infiltrated into the empty core. This usually changes the penetration depth of the propagating mode due to weaker refractive index contrast arising between core and cladding. Also, as the operation of solid-core PCF is ensured mostly by TIR over a broad range of communication bands, being only restricted by relatively loose interaction of the traveling signal with the analyte. The basic technique used in the fabrication of the PCF is somewhat matched with conventional fiber except in proper adjustment and

drawing of dielectric rods. The only difference that is put during fabrication is of monitoring of refractive index profile and its relative magnitude and distribution in the core and the cladding. The fabrication of PCF involves various methods, for example, outside vapor phase oxidation (OVPO), modified chemical vapor deposition (MCVD) method, vapor phase axial deposition (VAD), plasma-activated chemical vapor deposition [24]. All these methods ensure the uniformity and proper distribution of dielectric rods in the core and the cladding. These methods include fused silica (SiO_2) as normal glass materials for the synthesis of performing. The post-processing technique is used for stocking of these glasses. The effective refractive index of the core and the cladding in PCF is optimized by the use of appropriate doped material (GeO_2, P_2O_5, B_2O_3, etc.) during starting of the fabrication. The drawing tower reduces the outer diameter of silica rods from 20 μm to 1 μm. These reduced rods are stacked in different pattern and collapsed in silica glass by applying a vacuum tube machine. In our model; this will be arranged in a hexagonal array with a missing rod in the central region acting as a core with approximate outer diameter of ~10 μm. The perform containing other rods stacked around central missing rods will be elliptical is put in a silica tube with outer diameter of ~40 μm. These values are favorable for fast analyte infiltration and signal transport. An alternative way to optimize signal-analyte interaction without reducing core diameter too much is the incorporation of elliptical dielectric rods in lieu of circular dielectric rods, thus creating a micro-structured-asymmetric PCF. The elliptical dielectric rod of the cladding forces the propagating light to penetrate further into the analyte, and hereof increases the interaction of signal-analyte compared to symmetric PCF of the same dimension. The designed PCF, formed by omitting one central dielectric rods, contains a hollow core in which various biological analytes can be filled as point defects for their detection. The cladding of PCF consists of elliptical dielectric rods filled with plasma material. The background of the cladding is made of boron-doped normal silica material (see Fig. 1(a) and (b)). For most of the PCF sensor, the delivery of a high power laser beam is desirable, but it causes a change in the temporal and spectral shape of light. As the PBG guidance allows the use of an air-core, this structure has strong implications in reducing nonlinearity. Thus nonlinearity in this type of PCF does not come simply from the air-core. This PCF is capable of supporting guidance of approximately 99% of the optical mode in the air core.

propagating relatively undistorted than that of solid core index-guiding PCF. A tiny part of the guided mode (typically 1%), interacts with the surrounding glass, rendering significantly to Kerr nonlinearity. The structure can control the flow of the signal in the presence of multiple point defects created by analyte at the center of the hollow core. Although, in the hollow core, the majority of the light field (typically 99%) transmits in the absence of any material (in air-core). However, the light still feels interaction with surrounding glass wafer. This can be also imagined as if the light is constantly trying to tunnel the barrier developed between core and cladding, but continuously diverted back into the air-core. This phenomenon occurs due to the photonic bandgap effect generated between the core and the cladding of the PCF. The model illustrations of the field at different locations and index distribution for the different materials of this PCF have graphically been shown in Fig. 1(b). These illustrations supply an outstanding outfit for quantitative information about mode field distribution. To illustrate various characteristics of this PCF, the method we apply here is the finite-difference which is based on the straightforward solution to the exact eigenvalue equation for nonlinear wave propagation in the hexagonal core of PCF. The additional effort to make boundary-contoured meshes and the related issues of such meshes for execution require high precision while computation which is possible with the help of FDM. The FDM offers a very efficient and onward numerical tool to evolve a better understanding of RI sensing for different modes. This approach is applied for the packet of waves called soliton by taking a finite-difference of forward and backward propagating field in nonlinear wave equation traveling in PCF. This method uses discretization scheme for symmetric PCF and non-discretization scheme, for an asymmetric PCF (see Fig. 2). In both schemes, not only field is expanded, but the distribution of refractive index in the two-dimensional structure of PCF is also expanded by using Taylor expansion. The wave equation describing the guiding characteristics in PCF can be found by applying the transverse distribution of dielectric function in Maxwell equation. The corresponding governing wave equation concerning transverse distribution of electric field may be expressed as [25,26]

$$\frac{\partial^2 E_y(x,y)}{\partial x^2} + \frac{\partial}{\partial y}\left\{\frac{1}{[n_{x,y}(\lambda, I)]^2}\frac{\partial [n_{x,y}(\lambda, I)]^2}{\partial y}E_y(x,y)\right\} + \frac{\partial^2 E_y(x,y)}{\partial y^2} + \{K_0^2[n_{x,y}(\lambda, I)]^2 - \beta^2\}E_y(x,y) = 0 \quad (1)$$

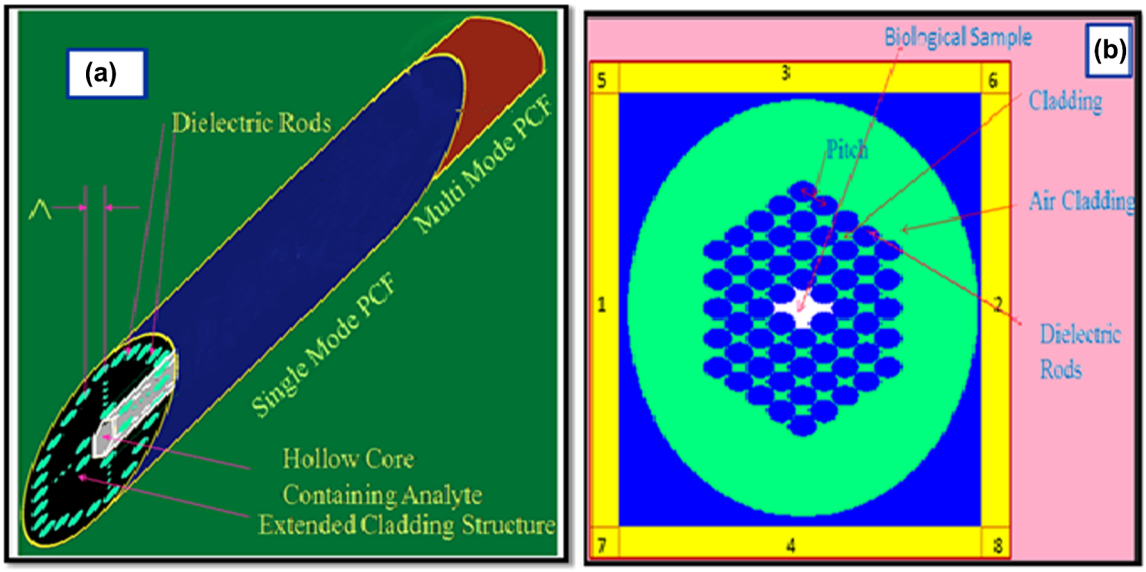

Fig. 1. (a) Geometrical structure of the designed hollow core PCF containing elliptical plasma dielectric rods and analyte in partially asymmetric core (b) Cross-sectional structure of the PCF containing the biological sample.

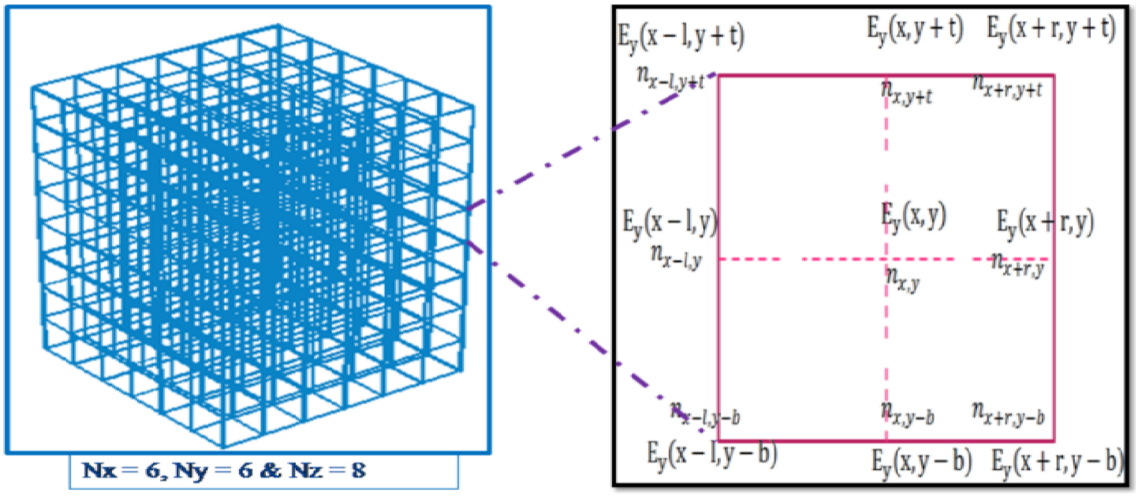

Fig. 2. The left part of the figure represents the structure of three-dimensional Yee grid and right part represents one small unit cell from Yee grid showing nondiscretization of field and refractive index for the asymmetric structure of designed PCF shown in Fig. (1).

$$n_{eff} = \frac{\beta}{K_0} \tag{2}$$

where $K_0 = \frac{2\pi}{\lambda}$ is the wave number in free space. The notation, $E_y(x,y)$ represents transverse field which is not constant but is the function of location. When it is in the core, then it's measurement will consider the refractive index of core, but when it is in cladding, then it measurement will also involve the interaction with plasma material and will generate cladding mode as mentioned numerically in Ref. [26]. The signal propagating in the core is used as a reference laser beam, and that filtering in cladding will constitute evanescent field which is used for biosensing application. The generation of the evanescent field depends on the refractive index of bioanalyte. The evanescent field is generated only for those analyte having the refractive index more than the effective refractive index of the cladding. For a lower refractive index of the analyte, no light is guided outside the band-gap. The other notations like, $n_{x,y}(\lambda, I)$ and β represent the refractive index at different locations of micro-structured PCF, as shown in Fig. 2, and propagation constant from which effective refractive index (n_{eff}) can be obtained by using the relation used in Ref. [27];

The n_{eff}, generally depends on the material used in drawing of PCF and mode developed in the cladding due to the evanescent field. In the presence of the analyte in the core and absorption of the signal in plasma dielectric rods, the light-guiding in cladding region will change, resulting in a change in n_{eff} also. In splicing of single-mode fiber with multiple modes, the voids at the joint position are collapsed. This results in the possible coupling between the signal propagating in the core & the evanescent field, with a strong field overlaps. In expression (1), the distribution of refractive indexes in chosen media i.e. cladding and dielectric rods is defined as [27,28],

$$n_{x,y}(\lambda, I) = \begin{cases} n_L(\lambda) + n_2(\lambda)I & \text{For cladding region} \\ \left(1 - \frac{\omega_p^2}{\omega^2 + i\gamma\omega}\right)^{1/2} & \text{For plasma dielectric rods} \end{cases} \tag{3}$$

where $n_L(\lambda)$ and $n_2(\lambda)$ are the linear and nonlinear parts of the refractive index whereas I represent the intensity of light. The linear variation of refractive index for different materials can be introduced by applying Sellmeier expression [28],

$$n_L(\lambda) = \sqrt{1 + \frac{B_1\lambda^2}{\lambda^2 - C_1} + \frac{B_2\lambda^2}{\lambda^2 - C_2} + \frac{B_3\lambda^2}{\lambda^2 - C_3}} \tag{4}$$

The coefficients in above expression are different for different molar percentages of doped materials. The nonlinear refractive index $n_2(\lambda)$ is proportional to real part of 3rd order susceptibility $\chi^3(-\omega, \omega, -\omega, \omega)$ defined as [29],

$$n_2(\lambda) = \frac{3}{4\varepsilon_0 c n_L} Re[\chi^3(-\omega, \omega, -\omega, \omega)] \tag{5}$$

To find the mode of Eq. (1), in the presence of various shape of dielectric rods and intensities of the Gaussian field, we apply finite difference computational method [30,31]. This method has been used because it can predict the results of such an arbitrary structure of micro order. In the implementation of this technique, we have the complex distribution of nonlinear processes in which Yee discretization scheme is used to interpret different components of the electric field in a rectangle which has been shown in Fig. 1(b). As the whole structure is superposed on the Yee grid, the cross point represents the field discontinuity propagating in PCF. For a Gaussian input field ($E_y(x, y) = E_0 \exp(x_0^2 - y_0^2) w_0^{-2}$), and refractive index distribution shown by Eq. (3), the finite difference equation for the governing Eq. (1) can be written as,

$$\begin{aligned} &\frac{2}{l(l+r)} E_0 \exp\left\{-\frac{[(x-1)^2 + y^2]}{w_0^2}\right\} + \frac{2}{r(l+r)} E_0 \exp\left\{-\frac{[(x+1)^2 + y^2]}{w_0^2}\right\} + \frac{2}{t(t+b)} \\ &\frac{2n_r^2(x, y-1)}{n_r^2(x, y) + n_r^2(x, y-1)} E_0 \exp\left\{-\frac{[x^2 + (y-1)^2]}{w_0^2}\right\} + \frac{2}{b(t+b)} \frac{2n_r^2(x, y+1)}{n_r^2(x, y) + n_r^2(x, y+1)} E_0 \\ &\exp\left\{-\frac{[x^2 + (y+1)^2]}{w_0^2}\right\} + \left(-\frac{2}{l(l+r)} - \frac{2}{r(l+r)} + \frac{2}{t(t+b)}\right. \\ &\left.\frac{2n_r^2(x, y-1)}{n_r^2(x, y) + n_r^2(x, y-1)} + \frac{2}{b(t+b)} \frac{2n_r^2(x, y+1)}{n_r^2(x, y) + n_r^2(x, y+1)} - \frac{4}{tb}\right) E_0 \\ &\exp\left[-\frac{(x^2 + y^2)}{w_0^2}\right] + \{K_0^2[n_{x,y}(\lambda, I)]^2\} E_0 \exp\left[-\frac{(x^2 + y^2)}{w_0^2}\right] = \beta^2 E_0 \exp\left[-\frac{(x^2 + y^2)}{w_0^2}\right] \end{aligned} \tag{6}$$

Here, micro-order lengths l, r, t, and b are varying from left to right and from top to bottom at different nodes of hypothetical mesh superimposed on the 2-D cross-sectional structure of PCF. In computation, these lengths scan the whole structure. Truncating these integers symmetrically about a center coordinate of PCF as it is appropriate for calculating mode, the Eq. (6) builds an ordinary eigenvalue problem. The form of full eigenvalue problem would appear like as,

$$[M_{i,j}] E_y(x, y) = (\beta)^2 E_y(x, y) \tag{7}$$

where $M_{i,j}$ is a Hermitian operator in which the indices *i* and *j* represent the arbitrary nodes points along x- and y-directions, respectively which are increasing from left to right and from top to bottom in the computational window. Computation time in calculating propagation constant in PCF is directly related to the number of discretized or non-discretization points. The analytical boundary condition is used at the

boundary of finite-difference cells. As the matrix shown by Eq. (7) is Hermitian, so by diagonalizing it, its eigenvalue means propagation constant (β) can be easily determined. The calculated β permits obtaining the RI sensing in signal transmission and the mode field area of PCF. The governing dispersion equation for PCF which shows its dependence on wavelength and intensity can be obtained from Refs. [28,31]. The Gaussian output field is obtained by calculating eigenvector corresponding to the eigenvalue of Eq. (7) which further gives effective area (A_{eff}) [27,31]. The last optical parameter that we find from the calculated values of n_{eff} is birefringence [32]. The expression for birefringence for the photonic band gap (PBG) guiding photonic crystal fibers (PCFs) governing nonlinear waves is modified by the not only intensity dependent effective refractive index of cladding but also due to trapping of the field in plasma rods. For multi-component glass, the refractive index of the cladding also depends on the concentration of different materials.

3. Sensor design & results discussion

This work demonstrates a highly sensitive hollow core PCF of asymmetric shape due to elliptical dielectric rods for sensing of analytes. The integration of such fiber-based device into on-chip frame incorporating capillary tubes for in- and out-flow of analytes into hollow core is one of the important issues for practical applications. Plasma dielectric rods, running along the length of the PCF, build new capacities for the proper interference between core guided mode and evanescent field, developed through gases or liquid in plasma dielectric rods. The designed PCF falls into the category of multimode device and is spliced with single mode device at both ends. The splicing of SMF and PCF is possible by repeated arc discharges through splicing machine at the ends of both the types of fibers after proper cleaving and alignment of the ends. The signal propagating in the core of single mode fiber is partially converted into cladding mode at splice region. The modes generated in the cladding get excited efficiently in this structure due to the light-matter interaction between plasma dielectric rods and biological samples lying in the hollow core. In case of sensing of human blood, formed in the hollow core can act as a diverging or converging medium due to their convex or concave shape of blood particles. This type of structure causes substantial refraction of the signal towards the adjacent ring of dielectric rods. Our finite difference approach allows calculating the effective refractive index in the periodic structure containing different dielectrics. The qualitative information can be obtained by computing eigenvector ($E_y(x,y)$) corresponding to each eigenvalue (β) of Eq. (6).

Fig. 3(a) and (b) represent, respectively, n_{eff} and dispersion curves for different pitch (Λ) of elliptical dielectric rods. Fig. 4 represents n_{eff} of hexagonal PCF for different semiminor axis of elliptical dielectric rods, and for different intensities of lunched laser light. Figs. 5, and 6 represent the dynamic shift in dispersion, and birefringence corresponding to the results of data used in the analysis of n_{eff}. Fig. 7(a), shows the n_{eff} of cladding modes for different analytes refractive indexes, the corresponding change in mode field area for reference beam is also shown in Fig. 7(b). Apart from the PCF dimensions considered so far, the basic parameters of the proposed sensor such as diameters of core, cladding, and air cladding are respectively set at 10, 40 & 41 μm. The forward and backward Taylor expansion of the field, $E_y(x,y)$ has been truncated at the fourth-order for getting accuracy in effective refractive index up to four decimal places. First, the analysis of the model with constant geometrical parameters and different concentration of boron has been performed to assess the influence of doped material on guiding characteristics in PCF. The Sellmeier coefficients for 3.5% doping of boron in silica have values [19] $B_1 = 0.6929642$, $B_2 = 0.4047468$, $B_3 = 0.9154064$, $C_1 = 0.003658351$, $C_2 = 0.01536631$, and $C_3 = 97.93383$, respectively. The value of third-order susceptibility in computation is $1.8\,V^2\,m^{-2}$ [29]. To design dispersion-compensating PBG PCF for sensing applications, a fiber with a relatively high asymmetric structure of dielectric-rods has been chosen for selective excitation and overlapping of core and cladding modes. The cladding mode is sensed by the optical spectrum analyzer, (OSA-HP86142A) and is regulated by the sensitivity of analyte, defect size, and shape of dielectric rods. The semimajor axis (a) of plasma dielectric rods has been kept constant with variation of semi-minor axis (b) for getting the effect of it on dispersion, birefringence and mode field area.

In the computation of effective refractive index, and field, the pulse width of the Gaussian input signal has been set at 3.0 μm. First, we investigate the dependence of n_{eff} and dispersion on the PCF structural parameter (pitch Λ). In our computation, a = 0.8 μm, and b = 0.3 μm, Λ is increased from 2.6 to 2.9 μm in a step of 0.1 μm whereas all other basic parameters are constant. The results have been shown in Fig. 3(a) and 3(b). In Fig. 3(a), n_{eff} of ≃1.4 is also close to mode guided in a normal glass fiber. However, even for this n_{eff}, guiding is possible by PBG due to structural difference between conventional PCF and our PCF containing the hollow core. Meanwhile, dispersion should be flattened for using PCF for PCF used in sensing applications. The results in Fig. 3, reveal that the effective refractive index of cladding can be dramatically tailored to obtain the dispersion in the desired range. Furthermore, the dispersion is also anomalous across most of the computation window. In general hollow core photonic band gap PCF, the small residual nonlinearity keeps a careful contradiction of self-phase modulation (SPM) and

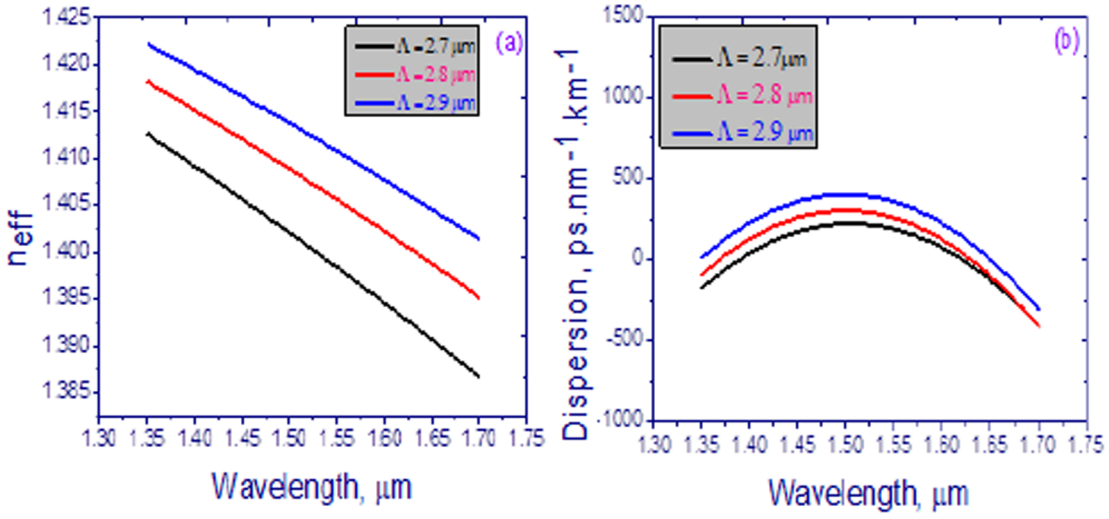

Fig. 3. Effective refractive index and dispersion versus wavelength curves for different filling factor of elliptical dielectric rods.

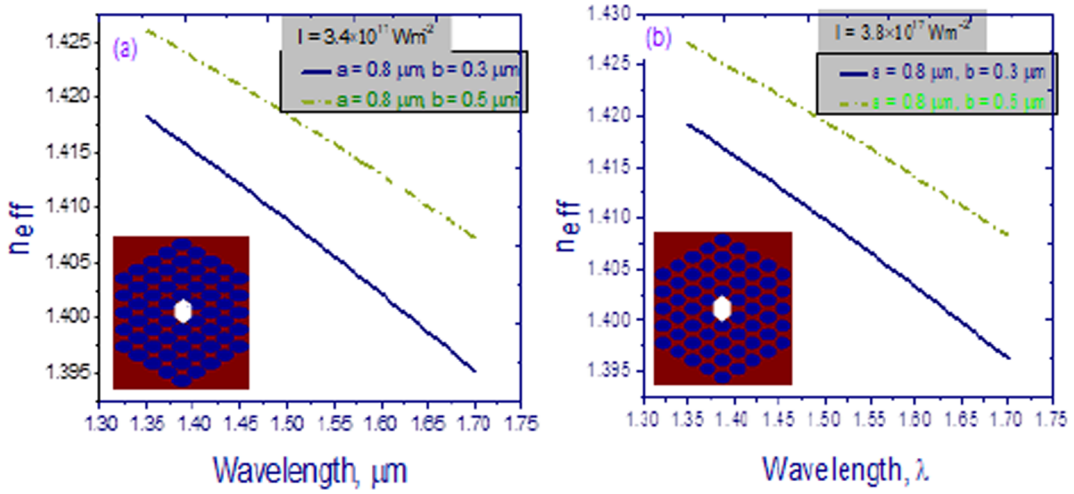

Fig. 4. Effective refractive index versus wavelength curves for different intensities and semiminor axis of elliptical dielectric rods.

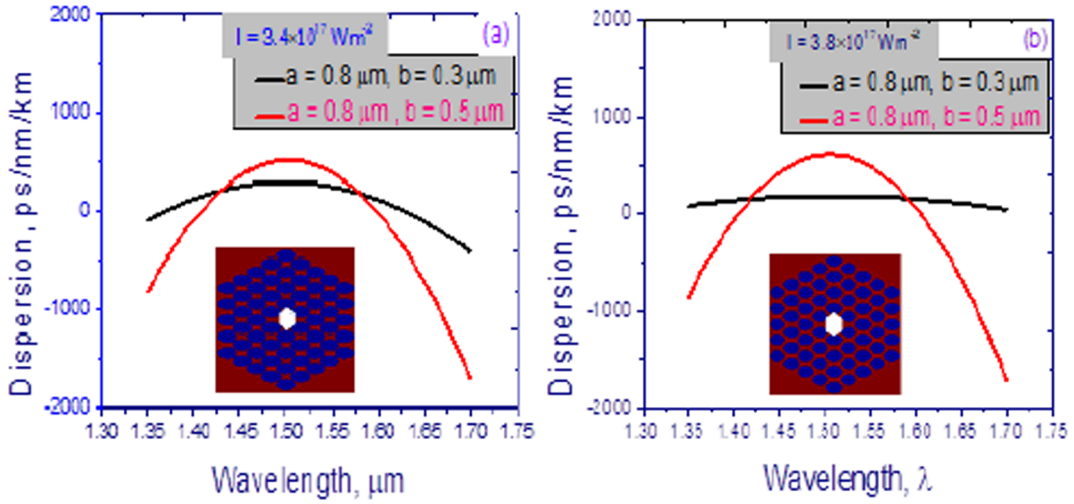

Fig. 5. Dispersion versus wavelength curves for different intensities and semiminor axis of elliptical dielectric rods.

anomalous group velocity dispersion by inducing a small amount of SPM. In general, the dispersion is flattened in the middle of the operating wavelength. However, for the same wavelength, the dispersion of our designed HCPCF with small pitch is more negatively flattened than that of the HCPCF with the large pitch. It means that dispersion will be more anomalous with the reduction of the distance between two dielectric rods. However, a minimal value of pitch will increase the difficulty of PCF drawing due to overlapping of dielectric rods. Therefore, there is a trade-off between dispersion play and PCF drawing feasibility.

We have also studied birefringence and mode field area for different design of elliptical dielectric rods and also for different intensities of the Gaussian signal. The design has been analyzed over E + S + C + L + U wavelength bands varying from 1.35 to 1.7 μm. The refractive index of plasma dielectric rods has been considered from Drude model [27] while the refractive index of differently doped material has been estimated from Sellmeier expression [28]. The distance between two adjacent dielectric rods, pitch $\wedge = 2.8$ μm has been chosen because these values give a better trade-off between an extension of flattened dispersion and effective mode field area of PCF.

In the designed PCF, the shape of elliptical dielectric rods of PCF has been considered to be of the different semiminor axis, but the other basic parameters of the fiber remain intact. The cladding modes have one of the unique properties of wavelength dependency of the refractive index of the analyte, and for the different optical response of the analyte in the core, and shape of dielectric rods, cladding will have different effective index profile. The presence of plasma dielectric rods in place of air-dielectric rods in the cladding region makes the PCF enable for measuring the change in concentration of bioliquid in hollow core. The PCF formed in this way follows the photonic band gap guiding mechanism, and the wave is trapped inside the core region. The nonlinearity causes the effective refractive index to shift toward higher value, dominating to a strong deviation in the dispersion of Gaussian beam and mode field area of PCF. From the n_{eff} versus λ curves shown in Fig. 4, it is clear that for the different contribution of plasma dielectric rods and intensities of the field, the slope of n_{eff} is normally different. The composition of the doped material and shape of dielectric rods may be used not only to obtain different values of n_{eff} for a reported wavelength range but also to get a particular slope of the curve at a particular wavelength to obtain the dispersion in the desired range.

Propagation constant depends on the physical properties of the materials and distribution of field in PCF and is actively connected with wavelength and intensity of the field. For a low filling factor of plasma dielectric rods, the contribution of dielectric rods material in RI sensing decreases giving n_{eff} close to that of background doped material for the fundamental mode. In another extreme, for a high filling factor of dielectric rods, n_{eff} approaches an index averaging of both materials. Dispersion is estimated by considering the fully transverse distribution of field in 2-D cross-sectional structure of fiber and adding the contribution of material dispersion calculated by Sellmeier expression to waveguide dispersion. Fig. 5 displays that PCFs, containing plasma

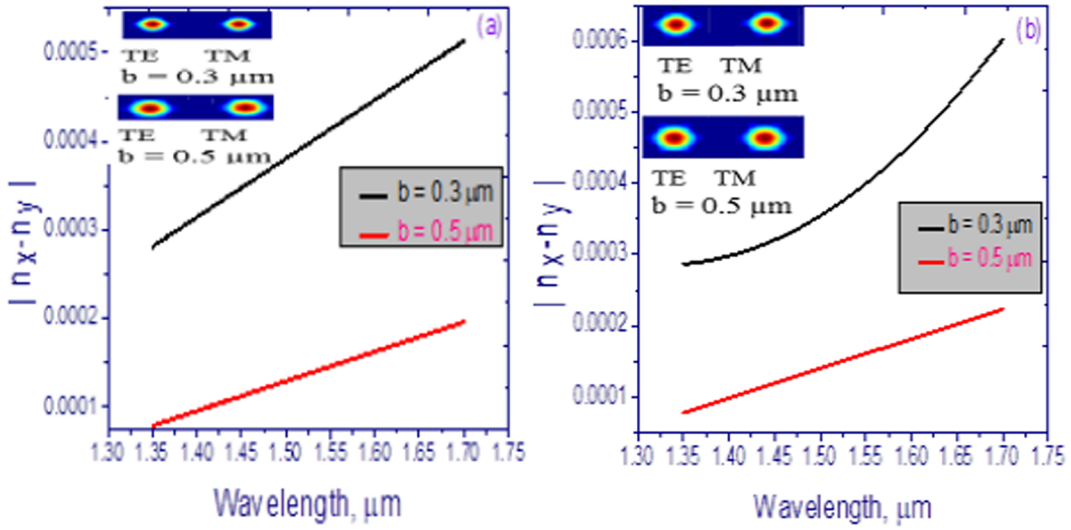

Fig. 6. Birefringence versus wavelength curves for different intensities and semiminor axis of elliptical dielectric rods. For both Figs. semiminor axis is 0.8 μm whereas for Fig. (a), I = 3.4 Wm^{-2} and for Fig. (b), I = 3.8 Wm^{-2}.

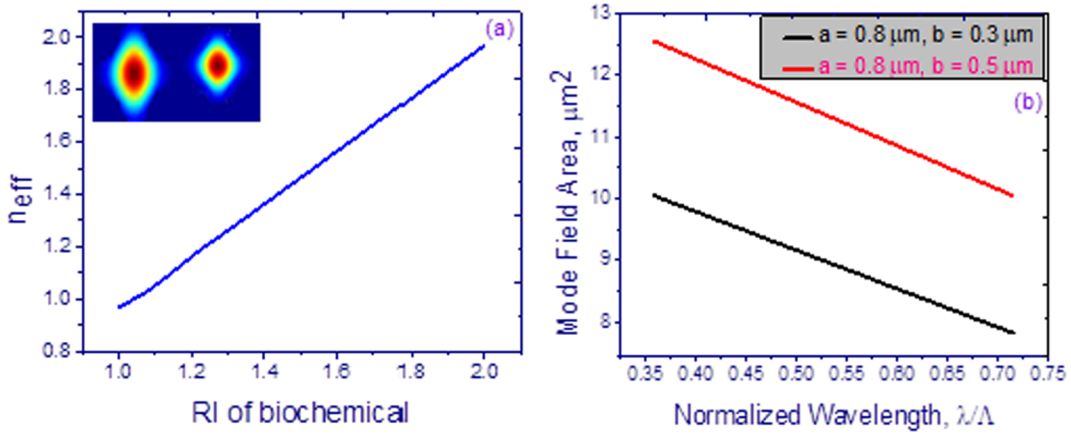

Fig. 7. (a) RI sensing curve and (b) mode field areas for different index of analytes.

dielectric rods have the prominent effect on dispersion slope and can be tuned to near zero dispersion by choosing proper shape and contribution of dielectric rods. The high filling factor of elliptical dielectric rods, as well as PCF having the hollow core of small diameter, can provide dispersion to be flattened near zero. The computational results reveal that dispersion for the highly asymmetric shape of dielectric rods having the semimajor axis, a = 0.8 μm, and semiminor axis, b = 0.3 μm has almost flattened tendency at low intensity but at high intensity, it is flattened at zero for the elevated filling factor of dielectric rods. The upward shifting of dispersion curves in Fig. 5 for the high filling factor of dielectric rods having the semiminor axis, b = 0.5 μm indicates a sizeable normal dispersion appearing in the middle of the operating wavelength. We can realize from these results that the PBG PCF, having the appropriate doping of boron have the potential to show large anomalous dispersion over the range of E + S + C + L + U wavelength band. This compensation of dispersion for intense pulse laser is not seen in normal PBG materials discovered in [20–23], and this model is a first indication to propagate a Gaussian signal of large pulse width into a small hexagonal core of size 10 μm without distortion.

The cladding modes can be increased by increasing the effective refractive index difference in the E_x- and E_y polarized modes. Meanwhile, the dielectric rods of designed PCF have been carefully tuned to optimize the birefringence in specific communication waveband. The curves in Fig. 6 show the effect of change of elliptical dielectric rods and intensities on birefringence. From these Figs., it is apparent that by proper selection of the semiminor axis of elliptical dielectric rods, it is possible to maintain low dispersion variation with high birefringence for E + S + C + L + U wavelength bands. The high birefringent PCF has high sensitivity due to their ability to enhance cladding mode. For asymmetric structure demonstrating the significant difference in two orthogonal polarization direction having the semimajor axis of 0.8 μm and the semiminor axis of 0.3 μm, the PCF fulfills the condition of the sensing operation. The inset of Fig. (6) provides an enlarged view of the TE and TM- polarization modes profile at 1.52 μm when b = 0.3 μm, and 0.5 μm. The asymmetric shape of field distribution and shifting towards outside the core support the results of dispersion and mode field area reported in Figs. 5, and 7. It can be seen that more optical power enters into the cladding region at the short semiminor axis.

Mode field area of PCF can be understood by getting field distribution at a particular propagation constant in the wavelength varying situation. Variation in propagation constant for varying intensities causes the change in field distribution in PCF which is determined in terms of mode field area (A_{eff}) and is calculated by using Eq. (7). For a Gaussian field, the definition of mode field area of PCF for the intense field can be extended to wavelength and intensity

dependent mode field area and can be expressed as $A_{eff} = \pi w^2(\lambda, I)$. The confinement of mode in core and cladding is directly proportional to mode field area. Analyzing the results of A_{eff}, shown in Fig. 7, one can notice that it shows nonlinear behavior at different wavelengths for the unusual shape of dielectric rods and intensities of the field. Out of these two types of PCF, the PCF for which dispersion is minimized with high birefringence can be used for analyte sensing. This can be done by inserting analyte in liquid form in the hollow core of PCF. When we add a high intensity laser pulse, then due to different index profiles of analytes, it will enhance the cladding modes. Fig. 7(a) and (b) show RI sensing of different analytes for the optimized structure of HCPCF in which semimajor axis is 0.8 μm and the semiminor axis is 0.3 μm. The other parameters, for example, core diameter, cladding diameter, optical parameter of selected materials are the same as reported in previous computations. The inset of Fig. 7(a) shows ingoing and outgoing field distribution at $w_0 = 3.0$ μm. The different analytes have different index profiles, and the corresponding n_{eff} will also be different. From the curves of Fig. 7(b) and inset curves of Fig. 7(a), it is also clear that for low index analytes, the field drives away of the core of the PCF resulting in higher values of mode field area and provides less confinement of beam in the core of HCPCF. Now, those for high index analytes, the field transposes into the core resulting in lower values of the mode field area with elevated confinement of field in the core of HCPCF.

4. Concluding remarks

Considerable effort has been constituted at our best to fully develop the hollow core PCF-based sensor containing suspended plasma dielectric rods in solid cladding for real-life applications. Notable, the existence of asymmetric shape of plasma dielectric rods enables the possibility of analyte detection in hollow core. The demarcation of dispersion profile, birefringence and mode field area for this type of nonlinear PCF is thoroughly investigated for pumping extended from 1.35 to 1.70 μm. For the proposed structure, we have determined the field confinement for TE- and TM- mode as a function of wavelength at various intense laser pulse and shape of plasma dielectric rods. Such a PCF confer a promising platform for refractive index sensing of analytes giving high birefringence with flattened dispersion near zero for semimajor axis, 0.8 μm and semiminor axis, 0.3 μm in communication wavelength bands varying from 1.35 μm to 1.70 μm. The RI sensing for different analytes reveals that core modes penetrate more in the cladding for chemicals showing low index profiles. However, for high index analytes, this sensor greatly enhances confinement of beam with approximately flattened dispersion for standoff nonlinear wave propagation.

Acknowledgments

This work was partially supported by the AICTE Collaborative Research Scheme, India through application ID 1-5730324531.

References

[1] Z. Hea, F. Tiana, Y. Zhua, N. Lavlinskaiab, H. Dua, Long-period gratings in photonic crystal fiber as an optofluidic label-free biosensor, Biosens. Bioelectron. 26 (2010) 4774–4778.
[2] E.K. Akowuah, I.E.E.E. Member, T. Gorman, H. Ademgil, S. Haxha, I.E.E.E. Senior Member, G.K. Robinson, J.V. Oliver, Numerical analysis of a photonic crystal fiber for biosensing applications, IEEE J. Quantum Electron. 48 (2012) 1403–1410.
[3] S. Tiwari, M.K. Singh, P.C. Pandey, Refractive index sensor based on spiral-shaped plastic optical fiber, IEEE Sens. J. 17 (2017) 1692–1695.
[4] A.A. Rifata, R. Ahmedb, A.K. Yetisenc, H. Buttb, A. Sabourib, G.A. Mahdirajie, S.H. Yunc, F.R. Mahamd Adikana, Photonic crystal fiber based plasmonic sensors, Sens. Actuators, B 243 (2017) 311–325.
[5] M.R. Hasan, I.E.E.E. Student Member, S. Akter, A.A. Rifat, S. Rana, K. Ahmed, R. Ahmed, H. Subbaraman, I.E.E.E. Member, D. Abbott, I.E.E.E. Fellow, Spiral Photonic crystal fiber-based dual-polarized surface plasmon resonance biosensor, IEEE Sens. J. 18 (2018) 133–140.
[6] B.K. Singh, M.K. Chaudhari, P.C. Pandey, Photonic and omnidirectional band gap engineering in one-dimensional photonic crystals consisting of linearly graded index material, J. Lightwave Technol. 34 (2016) 2431–2438.
[7] A.R. Hmmed, A. Rajib, K.Y. Ali, B. Haider, S. Aydin, G.A. Mahdiraji, S.H. Yunc, F.R.M. Adikana, Photonic crystal fiber based plasmonic sensors, Sens. Actuators, B 243 (2017) 311–325.
[8] L. Zhao-lun, H. Lan-tian, W. Wei, Tailoring nonlinearity and dispersion of photonic crystal fibers using hybrid cladding, Braz. J. Phys. 39 (2009) 50–54.
[9] A. Dixit, S. Tiwari, P.C. Pandey, Study of band structure of one-dimensional photonic crystal composed of dispersive and nonlinear dielectric materials, J. Mod. Opt. 64 (2017) 1240–1246.
[10] A. García, I. Sukhoivanov, J. Lucio, O. Manzano, I. Guryev, J. García, G. Ortiz, Numerical study of highly nonlinear photonic crystal fiber with tunable zero dispersion wavelengths, J. Electromagn. Anal. Appl. 07 (2015) 141–151.
[11] F. Belli, A. Abdolvand, J.C. Travers, P. St, J. Russell, Control of ultrafast pulses in a hydrogen-filled hollow-core photonic-crystal fiber by Raman coherence, Phys. Rev. A 97 (2018) 013814.
[12] H. Qu, M. Skorobogatiy, Resonant bio- and chemical sensors using low-refractive-index-contrast liquid-core Bragg fibers, Sens. Actuators, B 161 (2012) 261–268.
[13] C. Liu, W. Su, Q. Liu, X. Lu, F. Wang, T. Sun, P.K. Chu, Symmetrical dual D-shape photonic crystal fibers for surface plasmon resonance sensing, Opt. Express 26 (2018) 9039–9049.
[14] W.L. Ng, A.A. Rifat, W.R. Wong, G.A. Mahdiraji, F.R.M. Adikan, A novel diamond ring fiber-based surface plasmon resonance sensor, Plasmonics 13 (2018) 1165–1170.
[15] A.A. Rifat, K. Ahmed, S. Asaduzzaman, B.K. Paul, R. Ahmed, Development of photonic crystal fiber-based gas/chemical sensors, Computational Photonic Sensors (2019) 287–317.
[16] A. Yasli, H. Ademgil, Effect of plasmonic materials on photonic crystal fiber based surface plasmon resonance sensors, Modern Phys. Lett. B 33 (2019) 1950157.
[17] S. Chakma, M.A. Khalek, B.K. Paul, K. Ahmed, M.R. Hasan, A.N. Bahar, Gold-coated photonic crystal fiber biosensor based on surface plasmon resonance: design and analysis, Sens. Bio-Sens. Res. 18 (2018) 7–12.
[18] Q. Wenwen, L.Z. Chun, H. Shaoling, D. Xinyong, Z. Shuqin, Z. Zaixuan, J. Shangzhong, G. Jiangtao, W. Huifeng, High-sensitivity temperature sensor based on an alcohol-filled photonic crystal fiber loop mirror, Opt. Lett. 36 (2011) 1548–1550.
[19] P. Vladimir, Minkovich, B.S. Alexander, Tapered photonic crystal fibers coated with ultra-thin films for highly sensitive bio-chemical sensing, J. Eur. Opt. Soc.-Rapid Publ. 15 (2019) 7.
[20] S.K. Varshney, N.J. Florous, K. Saitoh, M. Koshiba, T. Fujisawa, Numerical investigation and optimization of a photonic crystal fiber for simultaneous dispersion compensation over S+C+L wavelength bands, Opt. Commun. 274 (2007) 74–79.
[21] M.A.R. Franco, V.A. Serrão, F. Sircilli, Microstructured optical fiber for residual dispersion compensation over S+C+L+U wavelength bands, IEEE Photon. Technol. Lett. 20 (2008) 751–753.
[22] J.P. Silva, D.S. Bezerra, V.F.R. Esquerre, I.E. Fonseca, H.E.H. Figueroa, Ge-doped defect-core microstructured fiber design by genetic algorithm for residual dispersion compensation, IEEE Photon. Technol. Lett. 22 (2010) 1337–1339.
[23] D.C. Tee, M.H. Abu Bakar, N. Tamchek, F.R.M. Adikan, Photonic crystal fiber in photonic crystal fiber for residual dispersion compensation over E + S + C + L + Uwavelength bands, IEEE Photon. J. 5 (2013) 7200607–7200615.
[24] N. Niizeki, et al., Recent progess in glass fiber in optical communication, Jpn. J. Appl. Phys. 20 (1981) 1347–1360.
[25] K. Kawano, T. Kitoh, Finite difference methods, Introduction to Optical Waveguide Analysis, John Wiley and Sons Inc., New York, 2001, pp. 117–165.
[26] E.K. Akowuah, T. Gorman, H. Ademan, S. Haxha, G.K. Robision, J.V. Oliver, Numerical analysis of a photonic crystal fiber for biosensing applications, IEEE J. Quantum Elect. 48 (2012) 1403.
[27] A. Dixit, S. Tiwari, P.C. Pandey, Optical properties of 3rd order Kerr hexagonal nonlinear photonic crystal fiber containing metal, Int. J. Mod. Phys. B 31 (2017) 1750047–1750056.
[28] G.P. Agrawal, Introduction, Pulse propagation in fibers, Nonlinear Fiber Optics, New York, 2007, pp. 1–50.
[29] X. Zhu, S. Li, Y. Du, Y. Han, W. Zhang, Y. Ruan, H.E. Heidepriem, S. Afshar, T. Monro, High stability supercontinuum generation in lead silicate SF57 photonic crystal fibers, Chin. Phys. B 22 (2013) 014215–014219.
[30] J. Sultana, M.S. Islam, K. Ahmed, A. Dinovitser, B.W.-H. Ng, D. Abbott, Terahertz detection of alcohol using a photonic crystal fiber sensor, Appl. Opt. 57 (2018) 2426–2433.
[31] A. Bjarklev, J. Broeng, A.S. Bjarklev, Theory and modelling of microstructured fibers, Photonic Crystal Fibres, Springer, Kluwer, 2003, pp. 90–96.
[32] Y. Chen, Q. Han, W. Yan, Y. Yao, T. Liu, Magnetic-fluid-coated photonic crystal fiber and FBG for magnetic field and temperature sensing, IEEE Photon. Technol. Lett. 28 (2016) 2665–2668.